ACS OMEGA

http://pubs.acs.org/journal/acsodf

Article

Tunable Anomalous Scattering and Negative Asymmetry Parameter in a Gain-Functionalized Low Refractive Index Sphere

Rfaqat Ali*

Cite This: *ACS Omega* 2022, 7, 2170−2176

Read Online

ACCESS | Metrics & More | Article Recommendations

ABSTRACT: Usually, low refractive index passive spheres exhibit strong forward scattering and a positive asymmetry parameter due to weak interference between the electric and magnetic scattering channels. In this work, we investigate, analytically and numerically, the forward scattering of light by a gain-functionalized low refractive index dielectric sphere. It is shown that by tuning the optical gain one can optimize the interference, which provides a novel paradigm to achieve the zero forward scattering and negative asymmetry parameter even for a low refractive index sphere. As a result, a low-density collection of such identical back scatterers provides an anomalous regime, where the scattering mean free path and extinction mean free path are greater than the transport mean free path. Furthermore, we also provide the numerical guideline to achieve the larger extinction mean free path without achieving preferential back-scattering.

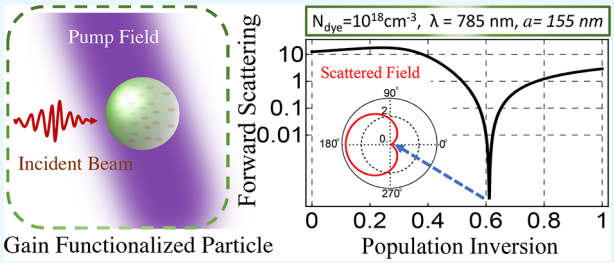

INTRODUCTION

The scattering of light by an individual subwavelength spherical particle has remained a subject of great interest with fundamental importance for the understanding of light−matter interaction with countless applications.[1−4] One of the most desired scientific goals in the optical scattering problem is to dictate the scattered field distribution around the particle.[5,6] The optimal control on the direction of scattered momentum is a matter of interest in light-emitting and light-guiding devices[7,8] and optical manipulation.[9−12] The direction of scattered light by a spherical particle can accurately be determined in terms of material properties and the length scale involved in the course of interaction[13,14] using the Mie scattering theory.[15]

With this perspective, the direction of the scattered light by a spherical particle can be explained using the asymmetry parameter (g), which is the average cosine of all scattering angles and is given as $g \equiv \langle \cos\theta \rangle$,[13,14] where θ is the angle between the incident wavevector to the scattered wavevector. For instance, a scatterer with $g = 1$ exhibits zero back-scattering, and $g = -1$ leads to zero forward scattering, which are the so-called first and second Kerker's conditions,[16] respectively. According to Kerker's criterion, the extremum values of the asymmetry parameter, $g = \pm 1$, can be achieved for magnetic spheres. In contrast, the electromagnetic scattering by a usual nonmagnetic dielectric sphere is elongated in the forward direction, and hence the asymmetry parameter is expected to be $1 > g > 0$. However, as a spacial case, $g = 0$ can be achieved for a dipole-like scattering. However, by considering a large refractive index sphere and composite sphere, one can achieve zero backward scattering with $g \approx 1$, which occurs due to induced magnetic dipoles owing to the rotation of displacement currents inside the sphere.[17−20] On the contrary, the second Kerker's condition hardly occurs in ordinary nonmagnetic scatterers due to the fundamental restriction imposed by the optical theorem. To be more specific, the observation of the second Kerker's condition not only is challenging but also is considered to be impossible to observe for the passive sphere, as required by causality.[21]

In the past two decades, some works have been reported demonstrating the negative asymmetry parameter by a magnetic sphere,[22] a sphere with large refractive index,[19,20,23,24] a plasmonic passive sphere,[25] and an active nanoparticle with a large refractive index.[26−28] In addition, the negative asymmetry parameter is also achieved by applying an external magnetic field[29] and in a cluster made of short-range correlated identical scatterers.[30] Nevertheless, to the best of our knowledge, no study has been proposed presenting a negative or turntable asymmetry parameter in a low refractive index sphere, especially in the visible frequency range.[31]

The negative asymmetry parameter plays a key role in many applications, where the switching of the scattered light direction is not only required but also should be achieved with optimal

Received: October 12, 2021
Accepted: December 21, 2021
Published: January 7, 2022

control. For instance, the structural information on a random medium consisting of a dilute dispersion of identical spheres can be extracted by means of unusual characteristic parameters, such as extinction mean free path (EMFP), scattering mean free path (SMFP), and transport mean free path (TMFP), denoted by l_{ext}, l_s, and l_t, respectively. The EMFP describes the attenuation of the averaged field inside the medium, which is equal to the SMFP for a lossless medium. Moreover, the EMFP and SMFP can be defined in terms of the TMFP and the average single particle scattering properties such as extinction efficiency, Q_{ext}, scattering efficiency, Q_s, and the asymmetry parameter.[32]

With this perspective, the negative asymmetry parameter plays a crucial role, and it may lead to an unusual multiple light-scattering regime, where the l_s becomes larger than the l_t. This achievement has important applications in many characterization and imaging methods such as the fabrication-tolerant broad-band operation of random spectrometers, where l_s and l_{ext} are needed to be larger than l_t.[33−35] A usual low refractive index sphere exhibits large forward scattering and positive g, which imposes severe limitations to achieve large values of l_{ext} and l_s.

In this work, we present an alternative strategy to achieve negative g, along with tunable EMFP and SMFP, by employing the optical gain in the visible frequency domain. We show that the gain-functionalized multipolar particle exhibits a preferential back-scattering which can be tailored experimentally, for instance, by tuning the power of the pump laser that governs the optical gain level. Furthermore, using a realistic gain model, we numerically (by Comsol multiphysics simulation) demonstrate that by varying the gain level inside the sphere, one can achieve zero forward scattering, even for a sphere of remarkably low refractive index compared to the ones reported so far.[31] As a result, for a low-density collection of such back-scattering identical scatterers, an anomalous regime occurs, where the EMFP becomes larger than the TMFP, that is, $l_{ext} > l_t$. In addition, we also propose an alternative strategy for tunable EMFP and show that by varying the optical gain level one can achieve the larger EMFP without relaying the negative g.

THEORETICAL MODEL

Let us consider an electromagnetic plane wave with vacuum wavelength λ_0 impinging on an isotropic nonmagnetic sphere of radius a, immersed in a non-absorbing medium of refractive index n. The Mie scattering theory provides the exact scattering solution to quantify the energy received from the incident field, energy scattered, and energy absorbed by the sphere in terms of extinction cross section C_{ext}, scattering cross section C_s, and absorption cross section C_a, respectively. As per convention, we normalize these cross sections by a geometric cross section of the sphere πa^2, which leads us to define normalized extinction and scattering and absorption efficiencies as[14]

$$Q_{ext} = C_{ext}/\pi a^2 = \frac{2}{x^2}\sum_{l=1}^{\infty}(2l+1)\mathrm{Re}(a_l + b_l) \tag{1}$$

$$Q_s = C_s/\pi a^2 = \frac{2}{x^2}\sum_{l=1}^{\infty}(2l+1)(|a_l|^2 + |b_l|^2) \tag{2}$$

and

$$Q_a = C_a/\pi a^2 = Q_{ext} - Q_s \tag{3}$$

respectively, where the index l denotes the lth order spherical harmonic, and $x = ka$ is the size parameter in the surrounding medium with $k = 2\pi/\lambda$, where $\lambda = \lambda_0/n$. In addition, a_l and b_l are the Mie scattering coefficients that can be calculated by applying the subsidiary boundary conditions at the sphere surface and given as[14,36]

$$a_l = \frac{m\psi_l(mx)\psi_l'(x) - \mu_s\psi_l(x)\psi_l'(mx)}{m\psi_l(mx)\xi_l'(x) - \mu_s\xi_l(x)\psi_l'(mx)} \tag{4}$$

$$b_l = \frac{\mu_s\psi_l(mx)\psi_l'(x) - m\psi_l(x)\psi_l'(mx)}{\mu_s\psi_l(mx)\xi_l'(x) - m\xi_l(x)\psi_l'(mx)} \tag{5}$$

where ψ_l and ξ_l are Riccati-Bessel functions and m and μ_s are the relative refractive index and relative permeability of the sphere, respectively. In the far-field domain, the scattered radiant intensity can be defined as

$$I(\theta, \phi) = I_1 + I_2 = \frac{1}{x^2}(|S_1(\cos\theta)|^2\sin^2\phi + |S_2(\sin\theta)|^2\cos^2\phi)$$

where I_1 and I_2 are the transverse electric ($\phi = 90°$) and transverse magnetic ($\phi = 0°$) components of the scattered intensity, respectively. In addition, θ and ϕ are the polar and the azimuthal angles, respectively. Furthermore

$$S_1(\cos\theta) = \sum_{l=1}^{\infty}\frac{2l+1}{l(l+1)}(a_l\pi(\cos\theta) + b_l\tau(\cos\theta)) \tag{6}$$

and

$$S_2(\cos\theta) = \sum_{l=1}^{\infty}\frac{2l+1}{l(l+1)}(a_l\tau(\cos\theta) + b_l\pi(\cos\theta)) \tag{7}$$

are the components of the scattering matrix,[14] where $\pi(\cos\theta)$ and $\tau(\cos\theta)$ describe the angular scattering patterns of the spherical harmonics.[14] Finally, the scattering efficiency in the forward direction ($\theta = 0$) is given as

$$Q_f = \frac{1}{x^2}\left|\sum_{l=1}^{\infty}(2l+1)(a_l + b_l)\right|^2 \tag{8}$$

It can be seen in eq 8 that the second Kerker's condition can be achieved by solving $\sum_{l=1}^{\infty}(2l+1)(a_l + b_l) = 0$, which presents multiple solutions for the Mie sphere. However, in the long wavelength region ($\lambda \gg a$) where only dipolar terms (a_1, b_1) are excited, $Q_f \simeq 0$ can be achieved by providing $a_1 \simeq -b_1$. This occurs when the condition $\epsilon_s = \frac{4-\mu_s}{2\mu_s+1}$ is satisfied, where ϵ_s is the relative permittivity of the sphere.[16,21,23,36] Otherwise for a nonmagnetic sphere the second Kerker's condition is difficult to achieve, as required by the optical theorem to preserve the causality.[21] It can be explained analytically by solving eq 8, where $Q_f = 0$ occurs only if $\sum_l \mathrm{Re}(a_l + b_l)$ and $\sum_l \mathrm{Im}(a_l + b_l)$ vanish simultaneously. However, for a passive sphere, real parts of a_l and b_l are obliged to be positive to preserve the passivity condition. Thus, sum of nonzero (positive) real scattering amplitudes can never be zero. These limitations can be circumvented by employing the optical gain in the sphere that would allow one to achieve negative $\mathrm{Re}(a_l)$ or $\mathrm{Re}(b_l)$. Thus, introduction of the optical gain is a necessary requirement to realize zero forward scattering.

Modeling of the Gain Media. The optical gain media can be designed by embedding the gain elements (e.g., fluorescent

https://doi.org/10.1021/acsomega.1c05662
ACS Omega 2022, 7, 2170−2176

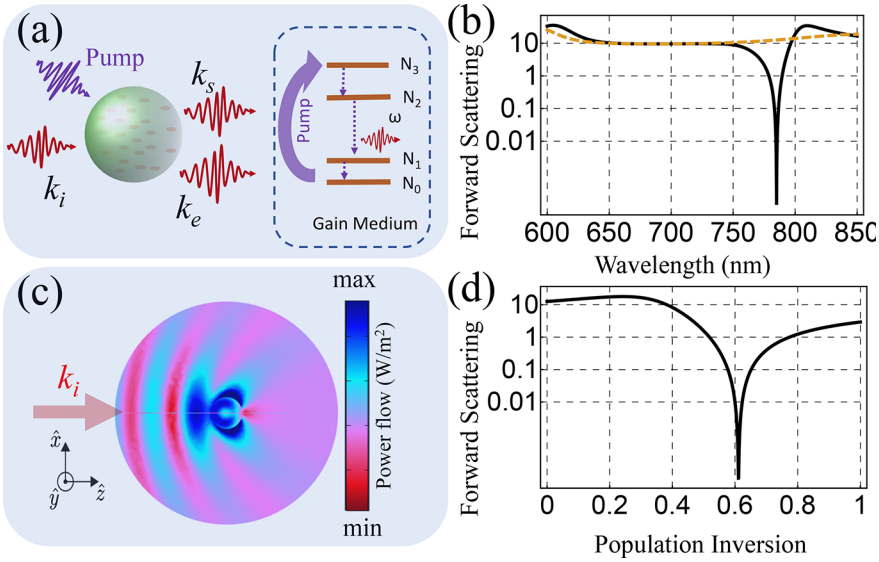

Figure 1. (a) Schematic illustration of problem: a dielectric sphere is doped with dye molecules. An incident beam and laser pump are illuminating the sphere, where k_i, k_s, and k_e are representing the wave vectors of the incident, scattered, and emitted light, respectively. In the inset, a four-level energy scheme is presented, where the laser pump with pump frequency higher than the probing frequency inverts the population of dye molecules. In this way, the excited dye molecules emit photons of frequency ω. (b) Forward scattering efficiency Q_f as a function of incident wavelength by a passive sphere $\tilde{N} = 0$ (dashed) and an active sphere $\tilde{N} = 0.61$ (solid). (c) Scattered field distribution around the particle for fixed $\tilde{N} = 0.61$ and $\lambda = 785$ nm. (d) Q_f as a function of population inversion for fixed wavelength at $\lambda = 785$ nm. In all calculations, the radius of the dielectric sphere and permittivity is fixed at $a = 155$ nm and $\epsilon_s = 6.7$, respectively.

dyes molecules or quantum dots) inside a host medium of permittivity ϵ_s. When the gain elements are excited by means of pump frequency, they emit photons due to their de-excitations, as shown in Figure 1a. As a result, close to the resonance frequency of the gain elements, the composite material shows a negative imaginary refractive index that characterizes the active nature of the composite particle under $\exp^{-i\omega t}$ monochromatic time-harmonic convention. For our purpose, we consider solvatochromic dye LDS 798 molecules[37,38] as a four-level atomic system, and each level has an occupation number density N_i, where $i = 0, 1, 2, 3$, as sketched in Figure 1a. The total number of dye molecules per unit volume of the host medium are represent by N_{dye} that can be given as $\sum_{i=0}^{3} N_i = N_{dye}$. As the incident pump laser excites the dye molecules from N_0 to N_3 during the de-excitation, they make a transition from the ith level to the jth level (ith> jth) with lifetime τ_{ij}, where $\tau_{21} \gg \{\tau_{32}, \tau_{10}\}$. Thus, frequency emitted due to the transition between the level 2 to level 1 would play a key role in the design of the gain media that we call probing frequency, as shown in Figure 1a. Finally, the effective permittivity of such a heterogeneous composite medium can be expressed by the following dispersion relation:[39−43]

$$\epsilon_{eff} = \epsilon_s + \frac{2N_{dye}\mu_d^2}{3\hbar\epsilon_0} \cdot \frac{\tilde{N}}{2(\omega - \omega_a) + i\Delta} \tag{9}$$

where $\omega = 2\pi c/\lambda$, c is the speed of light, $\Delta = 2/\tau$, τ is the relaxation time constant associated with energy relaxation processes of the dye molecules,[37,41] μ_d is the dipole moment transition amplitude of the dye molecules, ω_a is the emission frequency, $\hbar$ is the reduced Plank constant, and ϵ_0 represents the permittivity of free space. In addition, $\tilde{N}$ is the population inversion which is counted in terms of the number of dye molecules in the excited state. The population inversion $\tilde{N}$ can be controlled through the action of the external pump laser: for no pump, all dye molecules are in the ground state N_0 and hence $\tilde{N} = 0$; on the other hand, $\tilde{N} = 1$ can be achieved for a larger pump power that sets the all dye molecules in the excited state. By varying the pumping power, one can tune the gain level which allows the inferences between the electric and magnetic scattering amplitudes to be tailored. It is worth noting that the probing frequency ω is substantially different than the pump frequency (as sketched in Figure 1a); therefore, scattering contribution from the pump frequency can be blocked, thereby, we are not considering it in the Mie scattering calculations. Thus, the radiation pattern around the scatterer can be defined using the Mie scattering theory in terms of the asymmetry parameter:[14]

$$g = \langle \cos\theta \rangle = \frac{4}{Q_s x^2}\left(\sum_{l=1}^{\infty} \frac{l(l+2)}{l+1} Re(a_l a_{l+1}^* + b_l b_{l+1}^*) + \sum_{l=1}^{\infty} \frac{2l+1}{l(l+1)} \mathrm{Re}(a_l b_l^*)\right) \tag{10}$$

The multiple scattering theory of random media made of dilute concentrations of identical scatterers provides a connection between the l_t to the l_s and l_{ext} in terms of single particle scattering cross sections and asymmetry parameter. In this assumption, the average separation between the particles is considered to be significantly larger than the particle size without positional correlation. The relation between l_t and l_s of light in a such dilute medium is defined as[31,32]

$$l_t = \frac{l_s}{1 - g} \tag{11}$$

l_t and l_s can be defined in terms of transport cross section C_t and scattering cross sections C_s as[31,32]

$$l_t = 1/\rho C_t; \quad l_s = 1/\rho C_s$$

https://doi.org/10.1021/acsomega.1c05662
ACS Omega 2022, 7, 2170−2176

where ρ is the density of scatterers in the medium. As we are considering an active sphere and the absorption cross section of the sphere would be nonzero, therefore, it is worthwhile to discuss the absorption mean free path (l_a) which can be defined as $l_a = 1/\rho C_a$.[44,45] In this case, the EMFP should be different than the SMFP that can be expressed as $l_{ext}^{-1} = l_s^{-1} + l_a^{-1}$.[32,44,45] For the active media, it is more convenient to investigate the TMFP in terms of the EMFP and single particle scattering properties using the following relation:[25,31]

$$\frac{l_t}{l_{ext}} = \frac{Q_{ext}}{Q_{ext} - Q_s g} \tag{12}$$

It is clear that for a losses medium $C_a = 0$ and $l_{ext} = l_s$.

RESULTS AND DISCUSSION

In the following discussion, we consider gain-functionalized composite sphere composed of silicon carbide (SiC) as a host sphere of radius a = 155 nm, relative permittivity ϵ_s = 6.7 and doped with solvatochromic dye LDS 798 molecules[37] with a dye concentration N_{dye} as depicted in Figure 1a. The characteristic parameters of the dye molecules (appearing in eq 9) are given as $\omega_a = 2.42 \times 10^{15}$ Hz, $\mu_d = 1.33 \times 10^{-29}$ Cm, $\tau = 1 \times 10^{-14}$ s, and $N_{dye} = 1 \times 10^{18}$ cm^{-3}.[37,38,40,41] The effective refractive index m of the composite sphere is defined using eq 9 as $m = \sqrt{\epsilon_{eff}}$. Since m is a complex number which governs the optical properties of sphere, it behaves like a passive sphere if Im(m) $\geq$ 0 and active sphere otherwise. In the case of active sphere, the optical gain level can be tuned by varying the population inversion by means of an external pump laser, as depicted in Figure 1a, that governs the population inversion by exciting and de-exciting the dye molecules.

In Figure 1b, we demonstrate the forward scattering efficiency as a function of wavelength by a SiC sphere (dashed line) and an active sphere (black line) for fixed population inversion at $\tilde{N}$ = 0.61. It shows that the passive sphere presents large forward scattering for all wavelengths, and it is the ultimate fact that a sphere with a relatively lower refractive index ($m < 3$)[17,31] can never realize zero forward scattering due to limitations imposed by the optical theorem.[21,36]

Here, this limitation is circumvented by shining the pump laser to activate the dye molecules inside the SiC sphere and puts them into an excited state. In this scenario, we have additional photons (emitted photons) to meet the condition for causality during the suppression of forward scattering. As shown by the black line, the forward scattering is completely suppressed at a wavelength of λ = 785 nm.

In Figure 1c, we numerically, using Comsol, illustrate the angular distribution of the scattered field intensity at a fixed incident wavelength of 785 nm and $\tilde{N}$ = 0.61. It is clearly shown that the scattered field is elongated in the backward direction with zero footprint in the forward direction. In Figure 1d, we calculate Q_f as a function of population inversion, which shows that the required population inversion is not very sharp, and hence, one can experimentally control it by tuning the pump laser power.

It is important to emphasis that, here, Q_f = 0 is achieved in the presence of optical gain which optimizes the interference between the scattering coefficients. Particularly, the photons emitted by dye molecules amplify the field around the sphere, which is counted as negative absorption. Therefore, in this scenario, the real parts of the scattering amplitudes are expected to be negative, as given in Table 1, where the first six, three electric a_1, a_2, a_3 and three magnetic b_1, b_2, b_3, coefficients are

Table 1. Mie Scattering Coefficients of a Dye Functionalized Sphere with Radius a = 155 nm, Permittivity ϵ_s = 6.7 for Two Population Inversions ($\tilde{N}$ = 0 and $\tilde{N}$ = 0.61; Incident Wavelength Is Fixed at 785 nm)

$\tilde{N}$ = 0			
a_1	0.66140−0.47320i	b_1	0.77886 + 0.41501i
a_2	0.00503−0.07081i	b_2	0.00070−0.02649i
a_3	≃0−0.00250i	b_3	≃0−0.00046i
$\tilde{N}$ = 0.61			
a_1	+0.64911−0.79265i	b_1	−0.60615 + 0.95158i
a_2	−0.00814−0.07191i	b_2	−0.01532−0.01684i
a_3	−0.00034−0.00251i	b_3	−0.00023−0.00037i

given for a passive sphere and an active sphere. The forward scattering efficiency Q_f, in this case $1 \leq l \geq 3$, can be simplified as

$$Q_f = \frac{1}{x^2}((3(a_1 + b_1) + 5(a_2 + b_2) + 7(a_3 + b_3)) \tag{13}$$

For the passive sphere, all coefficients have positive real parts, and hence, a large Q_f is observed, whereas in the presence of photon emission, some of them appear to be negative; therefore, eq 13 gives Q_f = 0.

Figure 2a demonstrates the asymmetry parameter as a function of wavelength for a passive sphere (dashed line) and

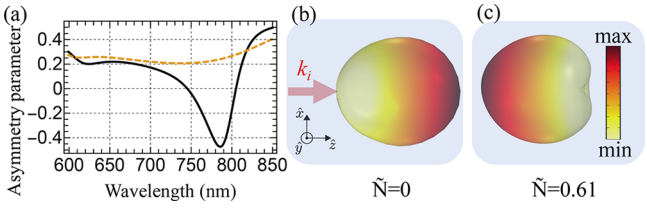

Figure 2. (a) Asymmetry parameter as a function of wavelength for a passive sphere, $\tilde{N}$ = 0 (dashed line), and active sphere, $\tilde{N}$ = 0.61 (solid line). (b) Corresponding scattered field intensity around the sphere for fixed population inversion at (b) $\tilde{N}$ = 0 and (c) $\tilde{N}$ = 0.61, where wavelength is 785 nm.

for an active sphere (black line). It shows that the asymmetry parameter is positive $g \simeq 0.2$ for the passive sphere due to preferential forward scattering, as shown in Figure 1b,d, and for active sphere $g \simeq -1/2$, which occurs due to the preferential back-scattering, as shown in Figure 1b−d. In Figure 2b,c, we numerically calculate the angular distribution of the scattered field for fixed population inversion $\tilde{N}$ = 0 and $\tilde{N}$ = 0.61, respectively. These three-dimensional scattering sketches illustrate that scattering is preferentially in the forward direction for the passive sphere and in the backward direction for the active sphere.

Until now, we have achieved the negative asymmetry parameter with zero forward scattering for a refractive index sphere relatively lower than that reported in ref 31. Consequently, it is easy to perceive that for all wavelengths corresponding to negative g, this should also lead to larger SMFP, that is, $l_s > l_t$. However, the EMFP also depends on Q_{ext} that might have negative values at a large gain level. Thus, only g cannot provide an exact description of l_t as a comparison to l_{ext}.

https://doi.org/10.1021/acsomega.1c05662
ACS Omega 2022, 7, 2170−2176

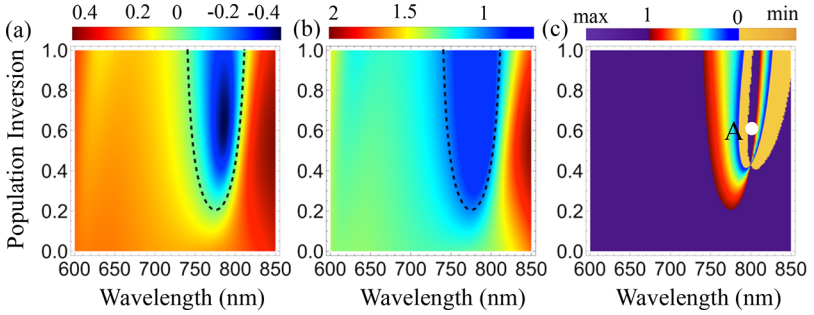

Figure 3. (a) Asymmetry parameter, (b) I_t/I_s, and (c) I_t/I_{ext} are plotted as a function of incident wavelength and population inversion, where the dotted line indicates (a) $g = 0$ and (b) $I_t/I_s = 1$. Here, radius and permittivity of the host sphere is $a = 155$ nm and $\epsilon_s = 6.7$.

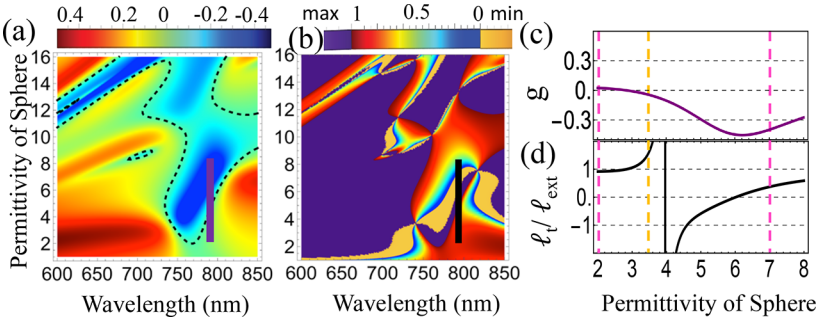

Figure 4. (a) Asymmetry parameter (the dotted line indicates $g = 0$) and (b) I_t/I_{ext} as a function of incident wavelength and permittivity of the sphere. We draw a purple line-cut in (a), black line-cut in (b) at wavelength $\lambda = 790$ nm along the permittivity axis. The corresponding asymmetry parameter and I_t/I_{ext} are plotted in (c) and (d), respectively, as a function of permittivity of the sphere for fixed wavelength $\lambda = 790$ nm. In this calculation, the radius of the sphere is taken at $a = 155$ nm and $\tilde{N} = 0.7$.

To this end, in Figure 3a, we plot the asymmetry parameter as a function of wavelength and population inversion, where the area enclosed by the dotted line corresponds to negative g, and the sphere exhibits zero forward scattering close to $g = -1/2$, as we have demonstrated in Figures 1 and 2. Figure 3b,c illustrates I_t/I_s and I_t/I_{ext}, respectively, as a function of wavelength and population inversion. It has been shown that the sphere with $g > 0$ and $g < 0$ leads to $I_t/I_s > 1$ and $I_t/I_s < 1$, respectively, as one can inspect from eq 11. Thus, the area enclosed by the dotted line leads to a parametric space where SMFP is larger than TMFP. On the contrary, I_t/I_{ext} is not necessarily less than 1 for all regions where the asymmetry parameter is negative. For instance, close to the transition length, $\lambda_a = 777$ nm, the low population inversion $\tilde{N} < 0.21$ provides weak photon emission, and we measure $I_t/I_{ext} > 1$. As the population inversion is increased, g becomes negative and $I_t/I_{ext} < 1$ is observed. However, we note that for certain wavelength and population inversion, where the emitted photons overcome the incident photons, in this scenario, the major scattering contribution is coming from the emission ones, and hence, according to eq 3, extinction efficiency becomes negative. For a better understanding of this fact, let us consider point A(800,0.61) in Figure 3c, where $g < 0$, $Q_{ext} < 0$, and $|Q_{ext} - Q_s g| < |Q_{ext}|$, which manifests as $I_t/I_{ext} > 1$ (further details are presented in Figure 5). Thus, the introduction of optical gain provides an additional degree of freedom to tune the EMFP without strictly depending on g and a large index sphere.

To gain further insight into the phenomenon, in Figure 4a, we present an asymmetry parameter as a function of wavelength and permittivity of the host dielectric sphere at fixed $\tilde{N} = 0.7$. It is clearly shown that the gain-functionalized sphere not only exhibits negative asymmetry parameter for lower permittivity sphere $\epsilon_s \simeq 2$ but also preferentially scatters light in backward directions at $\epsilon_s \simeq 5$, where $g = -1/2$. Here, the area enclosed by the dotted line indicates negative g, and in this region, $I_s > I_t$ should occur. In Figure 4b, we calculate I_t/I_{ext} as a function of wavelength and permittivity of the host sphere. It is clearly shown that for an active sphere, g and I_t/I_{ext} do not follow the fundamental rule as they do for a passive sphere.[25] To demonstrate the role of g on I_{ext}, we consider two lines in the parameter space of Figure 4a,b, and the corresponding g and I_t/I_{ext} are plotted in Figure 4c,d, respectively, versus permittivity of the host sphere. It is demonstrated that the sphere with $\epsilon_s = 2$ exhibits $g > 0$ and EMFP larger than TMFP (i.e., $I_{ext} > I_t$) as marked by a vertical dotted line. On the other hand, at $\epsilon_s = 3.5$, where $g < 0$ but EMFP is smaller than TMFP, $I_{ext} < I_t$, and at $\epsilon_s = 7$, $g < 0$ and $I_{ext} > I_t$, as indicated by the vertical dotted lines in Figure 4c,d. It is worth concluding that one can achieve tunable EMFP by employing the optical gain without strictly relying on negative g and a larger refractive index sphere. In this scenario, gain level and Q_{ext} play a crucial role in the tuning of mean free paths.

For deeper insights into this concept, now we are considering a sphere made of a low refractive index of 1.41 to unveil the role of gain on EMFP under the condition where g is positive. In Figure 5a, we calculate the asymmetry parameter as a function of wavelength and population inversion. The sphere has a low refractive index, and it presents a $g > 0$. In this case, it is immediately determined that the TMFP is large than the SMFP or $I_t/I_s > 1$. On the other hand, I_t/I_{ext} strongly depends on $\tilde{N}$ and wavelength, as shown in Figure 5b, where three distinct regions, A, $I_t/I_{ext} > 0$, B, $I_t/I_{ext} < 0$, and, C, $0 < I_t/I_{ext} < 1$, are found as

https://doi.org/10.1021/acsomega.1c05662
ACS Omega 2022, 7, 2170−2176

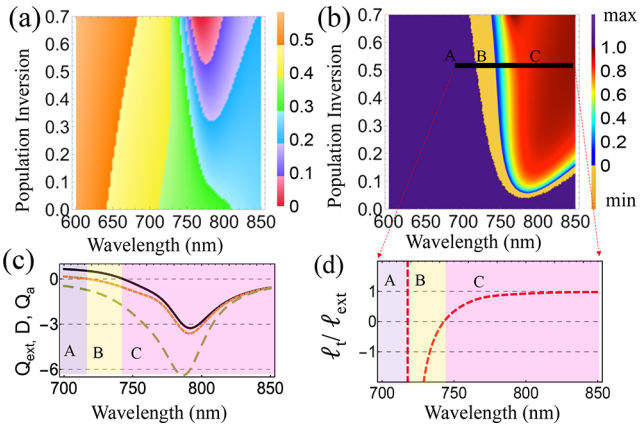

Figure 5. (a) Asymmetry parameter and (b) l_t/l_{ext} as a function of incident wavelength and population inversion. (c) Extinction efficiency (black line), denominator of eq 12 $D = (Q_{ext} - gQ_s)$ (dotted line) and absorption efficiency (dashed line) (d) l_t/l_{ext} as a function of permittivity for fixed population inversion $\tilde{N} = 0.5$ as marked by black lines in (b). Here, the radius of the sphere is taken at $a = 155$ nm and $\epsilon_s = 2$.

indicated in Figure 5b. To explore physical phenomena behind the scene, we draw a line at $\tilde{N} = 0.5$, which crosses through all of the regions, and we calculate the corresponding quantities such as Q_{ext} (black), denominator of eq 12, $D = (Q_{ext} - Q_s g)$ (dotted), and Q_a (dashed) are plotted in Figure 5c. In the first region A, where the sphere has a smaller gain level, the extinction efficiency and D are positive quantities, as shown in Figure 5c. Thus, it is found that $l_t > l_{ext}$, as shown in Figure 5d. In the second region B, gain level increases and the particle undergoes $Q_{ext} > 0$, and the electromagnetic field amplification governs the denominator of eq 12, such that it becomes negative. As a result, $l_t/l_{ext} < 0$ is measured and shown in Figure 5d. Finally, in region C, the sphere has achieved higher gain level such that the emitted photons overcome the incident photons and the extinction efficiency and D become negative, as shown in Figure 5c. As a result, in region C, $0 < l_t/l_{ext} < 1$ is measured and shown in Figure 5b,d. In a nutshell, it has been demonstrated that by applying the appropriate gain level, one can achieve the anomalous region where EMFP is larger than the TMFP without achieving the negative asymmetry parameter.

CONCLUSIONS

In conclusion, we have studied the electromagnetic scattering by a gain-functionalized low refractive index sphere. By providing a realistic optical gain model, we have, analytically and numerically (Comsol), shown that the implication of optical gain can optimize the destructive interference between the electric and magnetic scattering amplitudes. It has been demonstrated that optimal control on the optical gain level can not only achieve the negative asymmetry parameter but also completely offset the optical scattering in the forward direction by a strikingly low refractive index sphere than that reported to date. As a result, an anomalous regime occurs where the EMFP and SMFP are larger than the TMFP. Another novel finding of the presented work is the optimal control on EMFP, where we have shown that by tuning the experimentally controllable parameter (i.e., population inversion), one can achieve the large EMFP without necessarily achieving the negative asymmetry parameter. Altogether, we hope that our findings could provide a route to analyze the structural information on complex media and in the design of materials with specific transport properties.

AUTHOR INFORMATION

Corresponding Author

Rfaqat Ali − *Photonics Research Center, Applied Physics Department, Gleb Wataghin Physics Institute, University of Campinas - UNICAMP, Campinas, SP 13083-970, Brazil;* orcid.org/0000-0003-2612-4020; Email: rali.physicist@gmail.com

Complete contact information is available at: https://pubs.acs.org/10.1021/acsomega.1c05662

Notes

The author declares no competing financial interest.

ACKNOWLEDGMENTS

We thank S. Iqbal, G. Wiederhecker, F.A. Pinheiro, F.S.S. Rosa, and P.A.M. Neto for inspiring discussions. This work is partially supported by Fundacão de Amparo a Pesquisa do Estado de São Paulo (FAPESP) (2020/03131-2).

REFERENCES

(1) Novotny, L.; Hecht, B. *Principles of Nano-Optics*; Cambridge University Press, 2006.

(2) Curto, A. G.; Volpe, G.; Taminiau, T. H.; Kreuzer, M. P.; Quidant, R.; van Hulst, N. F. Unidirectional Emission of a Quantum Dot Coupled to a Nanoantenna. *Science* **2010**, *329*, 930−933.

(3) Dai, J.; Čajko, F.; Tsukerman, I.; Stockman, M. I. Electrodynamic effects in plasmonic nanolenses. *Phys. Rev. B* **2008**, *77*, 115419.

(4) Staude, I.; Pertsch, T.; Kivshar, Y. S. All-Dielectric Resonant Meta-Optics Lightens up. *ACS Photonics* **2019**, *6*, 802−814.

(5) Staude, I.; Miroshnichenko, A. E.; Decker, M.; Fofang, N. T.; Liu, S.; Gonzales, E.; Dominguez, J.; Luk, T. S.; Neshev, D. N.; Brener, I.; Kivshar, Y. Tailoring Directional Scattering through Magnetic and Electric Resonances in Subwavelength Silicon Nanodisks. *ACS Nano* **2013**, *7*, 7824−7832.

(6) Evlyukhin, A. B.; Novikov, S. M.; Zywietz, U.; Eriksen, R. L.; Reinhardt, C.; Bozhevolnyi, S. I.; Chichkov, B. N. Demonstration of Magnetic Dipole Resonances of Dielectric Nanospheres in the Visible Region. *Nano Lett.* **2012**, *12*, 3749−3755.

(7) Liu, W.; Miroshnichenko, A. E.; Neshev, D. N.; Kivshar, Y. S. Broadband Unidirectional Scattering by Magneto-Electric Core−Shell Nanoparticles. *ACS Nano* **2012**, *6*, 5489−5497.

(8) Novotny, L.; van Hulst, N. Antennas for light. *Nat. Photonics* **2011**, *5*, 83−90.

(9) Sáenz, J. J. Laser tractor beams. *Nat. Photonics* **2011**, *5*, 514−515.

(10) Ali, R.; Dutra, R. S.; Pinheiro, F. A.; Maia Neto, P. A. Enantioselection and chiral sorting of single microspheres using optical pulling forces. *Opt. Lett.* **2021**, *46*, 1640−1643.

(11) Ali, R.; Pinheiro, F. A.; Dutra, R. S.; Neto, P. A. M. Tailoring optical pulling forces with composite microspheres. *Phys. Rev. A* **2020**, *102*, 023514.

(12) Ali, R.; Pinheiro, F. A.; Dutra, R. S.; Rosa, F. S. S.; Maia Neto, P. A. Enantioselective manipulation of single chiral nanoparticles using optical tweezers. *Nanoscale* **2020**, *12*, 5031−5037.

(13) van de Hulst, H. C. Light scattering by small particles. *Quarterly Journal of the Royal Meteorological Society*; John Wiley and Sons: New York, 1958; Vol. *84*, pp 198−199.

(14) *Absorption and Scattering of Light by Small Particles*; John Wiley and Sons, Ltd., 1998; Chapter 4, pp 82−129.

(15) Mie, G. Contributions to the optics of turbid media, particularly of colloidal metal solutions. *Ann. Phys.* **1976**, *25*, 377−445.

(16) Kerker, M.; Wang, D.-S.; Giles, C. L. Electromagnetic scattering by magnetic spheres. *J. Opt. Soc. Am.* **1983**, *73*, 765−767.

(17) Kuznetsov, A. I.; Miroshnichenko, A. E.; Fu, Y. H.; Zhang, J.; Luk'yanchuk, B. Magnetic light. *Sci. Rep.* **2012**, *2*, 492.
(18) Ali, R. Lighting of a monochromatic scatterer with virtual gain. *Phys. Scr.* **2021**, *96*, 095501.
(19) Nieto-Vesperinas, M.; Sáenz, J. J.; Gómez-Medina, R.; Chantada, L. Optical forces on small magnetodielectric particles. *Opt. Express* **2010**, *18*, 11428−11443.
(20) García-Etxarri, A.; Gómez-Medina, R.; Froufe-Pérez, L. S.; López, C.; Chantada, L.; Scheffold, F.; Aizpurua, J.; Nieto-Vesperinas, M.; Sáenz, J. J. Strong magnetic response of submicron Silicon particles in the infrared. *Opt. Express* **2011**, *19*, 4815−4826.
(21) Alu, A.; Engheta, N. How does zero forward-scattering in magnetodielectric nanoparticles comply with the optical theorem? *Journal of Nanophotonics* **2009**, *4*, 1−18.
(22) Pinheiro, F. A.; Martinez, A. S.; Sampaio, L. C. New Effects in Light Scattering in Disordered Media and Coherent Backscattering Cone: Systems of Magnetic Particles. *Phys. Rev. Lett.* **2000**, *84*, 1435−1438.
(23) Lee, J. Y.; Miroshnichenko, A. E.; Lee, R.-K. Simultaneously nearly zero forward and nearly zero backward scattering objects. *Opt. Express* **2018**, *26*, 30393−30399.
(24) Geffrin, J. M.; García-Cámara, B.; Gómez-Medina, R.; Albella, P.; Froufe-Pérez, L. S.; Eyraud, C.; Litman, A.; Vaillon, R.; González, F.; Nieto-Vesperinas, M.; Sáenz, J. J.; Moreno, F. Magnetic and electric coherence in forward- and back-scattered electromagnetic waves by a single dielectric subwavelength sphere. *Nat. Commun.* **2012**, *3*, 1171.
(25) Varytis, P.; Busch, K. Negative asymmetry parameter in plasmonic core-shell nanoparticles. *Opt. Express* **2020**, *28*, 1714−1721.
(26) Xie, Y.-M.; Tan, W.; Wang, Z.-G. Anomalous forward scattering of dielectric gain nanoparticles. *Opt. Express* **2015**, *23*, 2091−2100.
(27) Shen, F.; An, N.; Tao, Y.; Zhou, H.; Jiang, Z.; Guo, Z. Anomalous forward scattering of gain-assisted dielectric shell-coated metallic core spherical particles. *Nanophotonics* **2016**, *6*, 1063−1072.
(28) Olmos-Trigo, J.; Sanz-Fernández, C.; Abujetas, D. R.; Lasa-Alonso, J.; de Sousa, N.; García-Etxarri, A.; Sánchez-Gil, J. A.; Molina-Terriza, G.; Sáenz, J. J. Kerker Conditions upon Lossless, Absorption, and Optical Gain Regimes. *Phys. Rev. Lett.* **2020**, *125*, 073205.
(29) Arruda, T. J.; Martinez, A. S.; Pinheiro, F. A. Electromagnetic energy and negative asymmetry parameters in coated magneto-optical cylinders: Applications to tunable light transport in disordered systems. *Phys. Rev. A* **2016**, *94*, 033825.
(30) Rojas-Ochoa, L. F.; Mendez-Alcaraz, J. M.; Sáenz, J. J.; Schurtenberger, P.; Scheffold, F. Photonic Properties of Strongly Correlated Colloidal Liquids. *Phys. Rev. Lett.* **2004**, *93*, 073903.
(31) Gómez-Medina, R.; Froufe-Pérez, L. S.; Yépez, M.; Scheffold, F.; Nieto-Vesperinas, M.; Sáenz, J. J. Negative scattering asymmetry parameter for dipolar particles: Unusual reduction of the transport mean free path and radiation pressure. *Phys. Rev. A* **2012**, *85*, 035802.
(32) Carminati, R.; Sáenz, J. J. Density of States and Extinction Mean Free Path of Waves in Random Media: Dispersion Relations and Sum Rules. *Phys. Rev. Lett.* **2009**, *102*, 093902.
(33) Noginov, M. A.; Novak, J.; Grigsby, D.; Zhu, G.; Bahoura, M. Optimization of the transport mean free path and the absorption length in random lasers with non-resonant feedback. *Opt. Express* **2005**, *13*, 8829−8836.
(34) Bret, B. P. J.; Couto, N. J. G.; Amaro, M.; Nunes-Pereira, E. J.; Belsley, M. Controllable transport mean free path of light in xerogel matrixes embedded with polystyrene spheres. *Opt. Express* **2009**, *17*, 6975−6981.
(35) Bahoura, M.; Noginov, M. A. Determination of the transport mean free path in a solid-state random laser. *J. Opt. Soc. Am. B* **2003**, *20*, 2389−2394.
(36) Ali, R. Revisit of generalized Kerker's conditions using composite metamaterials. *Journal of Optics* **2020**, *22*, 085102.
(37) Doan, H.; Castillo, M.; Bejjani, M.; Nurekeyev, Z.; Dzyuba, S. V.; Gryczynski, I.; Gryczynski, Z.; Raut, S. Solvatochromic dye LDS 798 as microviscosity and pH probe. *Phys. Chem. Chem. Phys.* **2017**, *19*, 29934−29939.
(38) Ali, R; Dutra, R S; Pinheiro, F A; Maia Neto, P A Gain-assisted optical tweezing of plasmonic and large refractive index microspheres. *Journal of Optics* **2021**, *23*, 115004.
(39) De Luca, A.; Ferrie, M.; Ravaine, S.; la Deda, M.; Infusino, M.; Rashed, A. R.; Veltri, A.; Aradian, A.; Scaramuzza, N.; Strangi, G. Gain functionalized core−shell nanoparticles: the way to selectively compensate absorptive losses. *J. Mater. Chem.* **2012**, *22*, 8846−8852.
(40) Polimeno, P.; Patti, F.; Infusino, M.; Sánchez, J.; Iatí, M. A.; Saija, R.; Volpe, G.; Maragó, O. M.; Veltri, A. Gain-Assisted Optomechanical Position Locking of Metal/Dielectric Nanoshells in Optical Potentials. *ACS Photonics* **2020**, *7*, 1262−1270.
(41) Pezzi, L.; Iatí, M. A.; Saija, R.; De Luca, A.; Maragó, O. M. Resonant Coupling and Gain Singularities in Metal/Dielectric Multishells: Quasi-Static Versus T-Matrix Calculations. *J. Phys. Chem. C* **2019**, *123*, 29291−29297.
(42) Veltri, A.; Chipouline, A.; Aradian, A. Multipolar, time-dynamical model for the loss compensation and lasing of a spherical plasmonic nanoparticle spaser immersed in an active gain medium. *Sci. Rep.* **2016**, *6*, 33018.
(43) Passarelli, N.; Bustos-Marún, R. A.; Coronado, E. A. Spaser and Optical Amplification Conditions in Gold-Coated Active Nanoparticles. *J. Phys. Chem. C* **2016**, *120*, 24941−24949.
(44) Meretska, M. L.; Uppu, R.; Vissenberg, G.; Lagendijk, A.; Ijzerman, W. L.; Vos, W. L. Analytical modeling of light transport in scattering materials with strong absorption. *Opt. Express* **2017**, *25*, A906−A921.
(45) García, P. D.; Smolka, S.; Stobbe, S.; Lodahl, P. Density of states controls Anderson localization in disordered photonic crystal waveguides. *Phys. Rev. B* **2010**, *82*, 165103.

https://doi.org/10.1021/acsomega.1c05662
ACS Omega 2022, 7, 2170−2176